Stretching of a confined ferrofluid: Influence of viscous stresses and magnetic field

Rafael M. Oliveira
Laboratório de Física Teórica e Computacional, Departamento de Física, Universidade Federal de Pernambuco, Recife, Pernambuco 50670-901 Brazil

José A. Miranda*
Department of Physics, University of Florida, P. O. Box 118440, Gainesville, Florida 32611-8440, USA
(Received 19 July 2005; revised manuscript received 6 February 2006; published 21 March 2006)

An analytical investigation is presented for the stretch flow of a viscous Newtonian ferrofluid highly confined between parallel plates. We focus on the development of interfacial instabilities when the upper plate is lifted at a described rate, under the action of an applied magnetic field. We derive the mode-coupling differential equation for the interface perturbation amplitudes and study both linear and nonlinear flow regimes. In contrast to the great majority of works in stretch flow we take into account stresses originated from velocity gradients normal to the ferrofluid interface. The impact of such normal stresses is accounted for through a modified Young-Laplace pressure jump interfacial boundary condition, which also includes the contribution from magnetic normal traction. We study how the stability properties of the interface and the shape of the emerging patterns respond to the combined action of normal stresses and magnetic field, both in the presence and absence of surface tension. We show that the inclusion of normal viscous stresses introduces a pertinent dependence on the initial aspect ratio, indicating that the number of fingers formed would be overestimated if such stresses are not taken into account. At early linear stages it is found that such stresses regularize the system, acting as an effective interfacial tension. At weakly nonlinear stages we verified that normal stresses reduce finger competition, which can be completely suppressed with the assistance of an azimuthal magnetic field. We have also found that the magnetic normal traction introduces a purely nonlinear contribution to the problem, revealing the key role played by the magnetic susceptibility in the control of finger competition.

DOI: 10.1103/PhysRevE.73.036309 PACS number(s): 47.54.−r, 47.20.Ma, 75.50.Mm, 68.35.Np

I. INTRODUCTION

Among nonequilibrium growth processes, the viscous fingering in Hele-Shaw cell has attracted much attention since its discovery by Saffman and Taylor [1]. The Saffman-Taylor instability occurs when a less viscous fluid pushes a more viscous one in pressure driven flow, resulting in the complex evolution of the fluid-fluid interface, and producing a wide range of interfacial patterns [2]. Stable smooth fingers are produced if the less viscous fluid is pumped from one side of a long rectangular channel [1,2]. Highly branched, fractal-like fronts are obtained if injection is performed through a hole at the center of the upper plate [2–4]. This famous interfacial instability belongs to the well-known family of Laplacian growth phenomena which includes diffusion limited aggregation, dendritic growth, and dielectric breakdown [5].

An alternative way for producing viscous fingering patterns is to stretch a very thin layer of a viscous fluid, sandwiched between two parallel plates, by lifting the upper plate while the lower one remains at rest. As the plates separate the outer less viscous fluid enters the system, and the more viscous inner fluid moves inward to conserve volume. As a result, the fluid-fluid interface deforms, forming visually striking patterns. In such a lifting version of the classic Saffman-Taylor problem the upper plate can be lifted from one end [6–9], or kept always parallel to the lower plate [10–17]. This last situation is somewhat simpler, in the sense that it induces a more uniform stretching where the plate spacing is just time dependent.

In recent years, the quest for other interesting pattern morphologies and even richer phenomenology resulted in a number of experimental and theoretical investigations of the uniform stretch flow in lifting Hele-Shaw cells [10–27]. If the fluids are immiscible and Newtonian [10,19–21,25–27] it is found that the initially circular droplet of the more viscous fluid undergoes a destabilization process via the penetration of multiple fingers of the outer, less viscous fluid. As time progresses these inward fingers become progressively thicker, while the left over branches of the more viscous fluid tend to form narrower fingers. At this stage, the interface behavior is markedly characterized by the competition among the fingers of the invading less viscous fluid, which advance towards the center of the droplet. At the same time, it is also observed that the outermost limit of the interface ceases to shrink, indicating that the competition among the narrower fingering structures of the more viscous fluid is suppressed. Following this period of intense instability and ramification, a second stage arises in which the number of fingered structures diminishes. In a final stage, near to the complete debonding of the plates, the droplet tends to shrink and recircularize. If the fluids are immiscible and non-Newtonian [11–15,19,22] various other morphological features may arise including the formation of highly ramified tree-like structures. Another interesting modifications assume

*On leave from Departamento de Física, LFTC, UFPE, Brazil. Email address: jme@df.ufpe.br

that the system involves miscible [17] or magnetic fluids [16,24].

When the fluids are Newtonian and immiscible numerical simulations of the lifting problem in time-dependent gap [10] show that increasingly smaller values of surface tension lead to stronger interface ramification, resulting in a delayed recircularization process. It has been also verified that when surface tension is absent, the penetrating fingers compete strongly, producing the incipient breakup of the contracting droplet, and ultimately leading to the formation of a topological singularity. Some important issues related to such singularity formation can be conveniently investigated by considering that the two fluids are miscible (zero interfacial tension situation). Highly accurate numerical simulations for miscible displacement in a time-dependent gap Hele-Shaw cell [17] show that the introduction of stresses arising as a result of concentration gradients at the diffusing interface may lead to dynamic surface tension-like effects. Such stresses (known as Korteweg stresses [28]) significantly affect the behavior of the mixing interface, introducing important stabilizing effects. In fact, it has been shown that singularity formation can be prevented by the action of stronger interfacial stresses.

In addition of being an intrinsically important academic problem, the lifting Hele-Shaw cell system is intimately related with the practical problem of adhesion [13,18–26]. A common parameter used for evaluating the effectiveness of an adhesive material is the time for which two plates separated by an adhesive can withstand the advance of viscous fingers, under constant load conditions [13]. Another possibility is to compute the force or energy required to pull one of the plates from the other, with constant drive speed [18–26]. There are recent evidence [13,20,25,26] that in both cases (constant pulling force or constant lifting velocity) the presence of the fingering instability may influence the adhesion between separating plates. The work by Thamida *et al.* [13] indicates that the adhesiveness of a confined fluid is strongly reduced (decrease of 50% relative to the case with no fingering) under constant load conditions, where the fingering instability tends to accelerate immediately to failure. In constant drive speed experiments [20,25,26] this reduction in adhesion is comparatively less intense, but still present notably for small initial plate separations. Other recent experimental and theoretical work at constant separation velocity [26,27] have found that the number of fingers predicted by ordinary linear analysis (based on Darcy's law and standard boundary conditions) is larger than the number obtained in the actual experiment [26,27]. The reason for this discrepancy is still an open and interesting question.

Based on our previous discussion, it is clear that it is very important to understand pattern formation in lifting Hele-Shaw cells, and study different ways of controlling emerging interfacial perturbations when the confined fluid is stretched. In order to examine possible ways of implementing effective controlling mechanisms in stretch flow, we consider the influence of a key factor that so far has been neglected: the effect of stresses acting normal to the contracting fluid-fluid interface. In fact, there is little consideration within the literature for the effect of hydrodynamic stresses in Hele-Shaw-type problems with immiscible fluids. Only very recently it has been shown [29,30], in the context of a constant gap-width rotating Hele-Shaw cell [31,32], that the incorporation of viscous stresses into the Young-Laplace pressure boundary condition results in important changes in the interface behavior as the gap spacing is allowed to vary. It means that key linear and nonlinear properties which determine the average number of emerging fingers, and finger competition dynamics are significantly affected as the gap spacing is modified. Evidently, this effect must be even more relevant in lifting Hele-Shaw flows, where the interface motion itself is driven by a gap-varying mechanism. Even though it seems obvious that viscous stresses should be taken into account in the description of pattern formation in variable-gap Hele-Shaw flows, a thorough investigation of this issue is lacking and still needs to be addressed. This is one of the main purposes of this work.

On the top of the effects of viscous stresses, we assume that the inner fluid is magnetic, or a ferrofluid [33,34]. These fluids behave superparamagnetically and can easily be manipulated with external magnetic fields that can act to either stabilize or destabilize the fluid interface. Here we investigate the situation in which the ferrofluid droplet evolves under the influence of a simple stabilizing magnetic field [35,36]. In an earlier work [16], restricted to the zero surface tension limit, and which completely ignored the effects of viscous and magnetic stresses, we have found theoretical evidence indicating that a magnetic field could be used to inhibit the emergence of cusp singularities in time-dependent gap Hele-Shaw flow. In this work, we go further and present a systematic study which investigates the combined role of interfacial stresses (both viscous and magnetic) and magnetic field in possibly controlling interfacial instabilities and singularities.

The paper is organized as follows: In Sec. II we introduce the formalism and obtain the weakly nonlinear equations describing flow of a ferrofluid in a variable-gap Hele-Shaw cell. The development of interfacial patterns is studied considering the influence of viscous and magnetic stresses, and the applied magnetic field. Section III discusses our linear stability results. At linear level we found that the inclusion of normal viscous stresses introduces a pertinent dependence on the gap width, indicating that the number of fingers formed would be overstimated if such stresses are not taken into account. In Sec. IV we show that some important morphological features of the interface like finger competition, can indeed be predicted and more quantitatively explained by our analytical, second-order mode-coupling approach. It is found that the magnetic contribution to the pressure jump boundary condition introduces a purely nonlinear effect into the problem, unveiling the important role played by the magnetic susceptibility in determining fingering dynamics at weakly nonlinear stages. It is verified that the interplay between normal stresses and azimuthal magnetic field may profoundly modify pattern evolution, providing effective mechanisms to control interfacial behavior in stretch flows. Our conclusions are summarized in Sec. V.

II. THEORETICAL APPROACH AND GOVERNING EQUATIONS

The geometry of the lifting cell problem is sketched in Fig. 1. Consider an incompressible ferrofluid of viscosity η

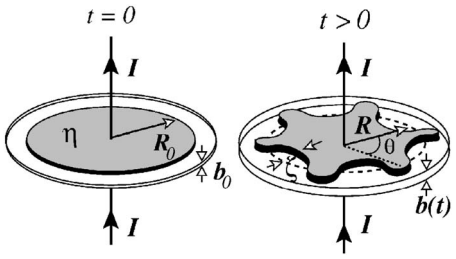

FIG. 1. Diagrammatic representation of the stretch flow of a ferrofluid (gray fluid) confined between parallel plates at $t=0$ (left) and $t>0$ (right). The azimuthal magnetic field is produced by a long, straight wire carrying an electric current I.

located between two narrowly spaced flat plates. The outer fluid is nonmagnetic, and of negligible viscosity. At time $t=0$ the droplet is circular and has initial radius R_0. The initial plate spacing is represented by b_0. At a given time $t>0$ the plate-plate distance is denoted by $b=b(t)$, and the droplet has a perturbed shape described as

$$\mathcal{R}(\theta,t) = R(t) + \zeta(\theta,t), \tag{1}$$

where

$$\zeta(\theta,t) = \sum_{n=-\infty}^{+\infty} \zeta_n(t)\exp(in\theta) \tag{2}$$

represents the net interface perturbation with Fourier amplitudes $\zeta_n(t)$, and discrete azimuthal wave numbers n. $R=R(t)$ is the time-dependent unperturbed radius of the shrinking ferrofluid interface. Conservation of ferrofluid volume leads to the useful relation $R^2b=R_0^2b_0$.

A long straight current-carrying wire of negligible radius is directed along the axis perpendicular to (coaxial with) the plates. The magnetic field produced is $\mathbf{H}=I/(2\pi r)\hat{\mathbf{e}}_\theta$, where r is the distance from the wire, I represents the electric current, and $\hat{\mathbf{e}}_\theta$ is a unit vector in the azimuthal direction. Note that the azimuthal symmetry and radial gradient of the magnetic field will result in a magnetic force directed radially inward [35,36]. This is one of the ways we use to stabilize the perturbed contracting interface.

To study the hydrodynamics of the system, the usual Navier-Stokes equation is modified through the inclusion of terms representing the magnetic effects. We follow the standard approximations used by Rosensweig [33] and others [34,37–39] and assume that the ferrofluid is magnetized such that its magnetization $\mathbf{M}$ is collinear with the applied field. When this is the case, the magnetic body force is given by $\mu_0 M\nabla H$, where μ_0 is the magnetic permeability of free space and H is the *local* magnetic field. The local magnetic field can include contributions from the applied field as well as the demagnetizing field. We consider only the lowest order effect of the magnetic interactions that would result in fluid motion. Thus, in the azimuthal field situation, we consider only the applied field in determining the magnetization $\mathbf{M}=\chi\mathbf{H}$, where χ is a constant magnetic susceptibility.

For the quasi-two-dimensional geometry of the Hele-Shaw cell, we reduce the three-dimensional (3D) flow to an equivalent two-dimensional one by averaging over the direction perpendicular to the plates. Using no-slip boundary conditions and neglecting inertial terms, one derives a modified Darcy's law as [39,40]

$$\mathbf{v} = -\frac{b^2}{12\eta}\nabla\Pi, \tag{3}$$

where ∇ denotes the two-dimensional gradient operator in polar coordinates (r,θ). The generalized pressure $\Pi=p-\Psi$ contains both the hydrodynamic pressure p and a magnetic pressure represented by a scalar potential $\Psi=\mu_0\chi H^2/2$. Since the observable quantities (like fluid velocity $\mathbf{v}$) are determined from gradients in Π, we take, without loss of generality, the generalized pressure of the outer fluid to be zero.

We now impose the incompressibility of the full three-dimensional flow, and take its average over the transversal direction to obtain a modified incompressibility condition [7]

$$\nabla\cdot\mathbf{v} = -\frac{\dot{b}(t)}{b(t)}, \tag{4}$$

where the overdot denotes total time derivative. From Eq. (4) it can be verified that the equation satisfied by the velocity potential ϕ ($\mathbf{v}=-\nabla\phi$) differs from Laplace equation valid in the usual case of constant gap, so that here the velocity potential is not a harmonic function. However, since the gap is only time dependent, the solution of the Poisson equation for ϕ can be conveniently expressed in terms of two contributions, namely $\phi=\phi_0+\bar{\phi}$, where $\bar{\phi}=\dot{b}r^2/(4b)$ is the radial particular solution, and ϕ_0 satisfies the Laplace equation [3,4].

In addition to the effects considered above, we still have to include other important contributions which result from the action of viscous and magnetic stresses. In order to do that, we consider a generalized Young-Laplace pressure jump boundary condition at the interface, which expresses the equilibrium condition on the normal component of the local stress tensor across the fluid-fluid interface [29,30,33,34,41–43]

$$\mathbf{n}\cdot\boldsymbol{\pi}\cdot\mathbf{n} = -\gamma\kappa + \tfrac{1}{2}\mu_0(\mathbf{M}\cdot\mathbf{n})^2, \tag{5}$$

where

$$\pi_{ik} = -p\,\delta_{ik} + \eta\left[\frac{\partial v_i}{\partial x_k} + \frac{\partial v_k}{\partial x_i}\right] \tag{6}$$

includes a viscous friction term proportional to η, δ_{ik} denotes the Kronecker delta function, and v_i represents the ith component of the ferrofluids' velocity vector. The first term at the right-hand side of Eq. (5) represents the usual contribution related to surface tension and interfacial curvature κ [1–4], with $\mathbf{n}=\nabla[r-\mathcal{R}(\theta,t)]/|\nabla[r-\mathcal{R}(\theta,t)]|$ denoting the unit normal vector at the interface. A noteworthy feature of Eq. (5) is the inclusion of a magnetic contribution to the interfacial stress balance (second term at the right hand side), the so-called magnetic normal traction [33,34], which considers the influence of the normal component of the magnetization at the interface.

By rewriting Eq. (6) in polar coordinates (r,θ), and substituting the resulting expression into the equilibrium condi-

tion Eq. (5), we obtain the pressure jump boundary condition at the interface

$$p = \gamma\kappa - \frac{1}{2}\mu_0(\mathbf{M}\cdot\mathbf{n})^2 - 2\delta\eta\frac{\partial^2\phi}{\partial r^2}. \tag{7}$$

For the current azimuthal field configuration the lowest order contribution of the magnetic normal traction term is given by $[\mu_0\chi^2 I^2/8\pi^2 R^4]\,(\partial\zeta/\partial\theta)^2$. Note that this magnetic piece is of second order in the interface perturbation ζ, being legitimately nonlinear and therefore of no influence at purely linear stages of interfacial evolution. The third term at the right-hand side of Eq. (7) takes into account viscous stresses originated from normal velocity gradients which are nonzero and of relevance to any radially symmetric Hele-Shaw flow. Equation (7) expresses that, if viscous stresses and magnetic interactions are accounted, the curvature term is balanced not only by pressure difference, but also by the normal components of the viscous stress ($\sim\partial v_r/\partial r$) and magnetization. Note that by "normal," we mean normal to the fluid-fluid interface, and *not* normal to the surface separating the ferrofluid and the upper plate. In the present high aspect ratio case (thin gap compared to any in-plane dimension), the flow between the plates is mostly horizontal and radial, such that the Darcy's law approach (for incompressible and immiscible Newtonian fluids) applies and viscous stresses acting along the transversal ($\sim\partial v_z/\partial z$) and tangential directions can be neglected. The parameter δ [$\delta=1$ ($\delta=0$) if normal stresses are (not) considered] is used to keep track of the contributions coming from the new term in Eq. (7) in our mode-coupling description. As we will verify below the addition of extra stresses in Eq.(7) introduces a pertinent dependence on the initial aspect ratio at both linear and weakly nonlinear stages [Eqs. (8)–(13)].

The problem is then specified by the generalized pressure jump boundary condition Eq. (7), plus the kinematic boundary condition, which states that the normal components of each fluid's velocity $\mathbf{v}_n = -\mathbf{n}\cdot\boldsymbol{\nabla}\phi$ are continuous at the interface. The tangential components, however, are discontinuous and give rise to a vortex sheet strength at the interface, where vorticity is concentrated. Even though the so-called vortex sheet formalism [44] is an useful alternative tool to describe interfacial dynamics in Hele-Shaw cells, the tangential velocity discontinuity plays no direct role in determining the pressure boundary condition (7) in our current problem. Here the strongest shear flow is along the radial direction. We define Fourier expansions for the velocity potentials, and use the boundary conditions to express ϕ in terms of ζ_n to obtain the *dimensionless* mode-coupling equation for the system (for $n\neq 0$)

$$\dot{\zeta}_n = \lambda(n)\zeta_n + \sum_{n'\neq 0}\left[F(n,n')\zeta_{n'}\zeta_{n-n'} + G(n,n')\dot{\zeta}_{n'}\zeta_{n-n'}\right], \tag{8}$$

where

$$\lambda(n) = \frac{1}{J(n)}\left\{\frac{1}{2}\frac{\dot{b}}{b}[|n| - J(n)] - \frac{\sigma b^2}{R^3}|n|(n^2-1) - |n|N_B\frac{b^2}{R^4}\right\} \tag{9}$$

denotes the linear growth rate, with

$$J(n) = \left[1 + \delta\frac{|n|(|n|-1)b^2}{6q^2R^2}\right], \tag{10}$$

where

$$q = \frac{2R_0}{b_0} \tag{11}$$

is the initial aspect ratio, and

$$F(n,n') = \frac{1}{RJ(n)}\left\{\frac{1}{2}\frac{\dot{b}}{b}\left[|n|\left(\mathrm{sgn}(nn') - \frac{1}{2}\right) - 1 + [J(n)-1]\times\left[\frac{3|n'| - n'^2 - 2}{|n|-1} + |n|\mathrm{sgn}(nn') - 1\right]\right] - \frac{\sigma b^2}{R^3}|n|\left[1 - \frac{n'}{2}(3n'+n)\right] + \frac{3}{2}|n|N_B\frac{b^2}{R^4}\left[1 + \frac{\chi}{3}n'(n'-n)\right]\right\}, \tag{12}$$

$$G(n,n') = \frac{1}{RJ(n)}\left\{|n|[\mathrm{sgn}(nn') - 1] - 1 + [J(n)-1]\times\left[\frac{3|n'| - n'^2 - 2}{|n|-1} + |n|\mathrm{sgn}(nn') - 1\right]\right\} \tag{13}$$

represent second-order mode-coupling terms. The sgn function equals ± 1 according to the sign of its argument. In Eq. (8) in-plane lengths, $b(t)$, and time are rescaled by $L_0 = 2R_0$, b_0, and the characteristic time $T = b_0/|\dot{b}(0)|$, respectively. The parameter $\sigma = \gamma b_0^3/[12\eta|\dot{b}(0)|L_0^3]$ denotes the dimensionless surface tension, and $N_B = \mu_0\chi I^2 b_0^3/[48\pi^2\eta|\dot{b}(0)|L_0^4]$ represents the dimensionless magnetic Bond number.

As mentioned earlier, note that the extra stress parameter $\delta=1$ [or equivalently, the function $J(n)$], originated from Eq. (7), introduces an important additional dependence of the linear growth rate $\lambda(n)$, and also of the mode-coupling terms $F(n,n')$ and $G(n,n')$ on the initial aspect ratio q. Note the presence of the magnetic field term N_B in both $\lambda(n)$ and $F(n,n')$, where the contribution from the magnetic normal traction appears in $F(n,n')$ as the term including the magnetic susceptibility χ. Among other things, this dependence on δ and N_B is required to an accurate description of the finger competition mechanisms in lifting Hele-Shaw flows. From now on, we work with the dimensionless version of the equations.

We close this section by pointing out an important requirement of the Darcy's law formulation we employed in this work: as is common in Hele-Shaw systems [17], we consider that during the lifting process the system remains of large aspect ratio: the gap width b is always far smaller than a characteristic length scale in the plane of the cell, which we

take as the droplet radius R, so that $R/b \gg 1$. Of course there are other theoretical approaches for the dynamics of fluids in the Hele-Shaw geometry which are free from such restriction. For example, under more general circumstances (not limited to the large aspect ratio requirement) the solution of full three-dimensional Stokes equations [43] or the Brinkman model [45–47] are probably more appropriate and accurate to describe patterns occurring in debonding. However, it is worth noting that such a more general description would involve a three-dimensional free boundary problem, where the interface position itself is an unknown which is part of the dynamics. So, there is no doubt that it would be a considerably challenging and difficult physical problem [27,46]. Therefore, the Darcy's model is still a very welcome and useful tool for exploring the current time-dependent gap Hele-Shaw problem, at least for sufficiently high aspect ratio.

Finally, we would like to call the reader's attention to another noteworthy point: note that, within the large aspect ratio assumption ($R/b \gg 1$), the corrections considered in Eqs. (5) and (6) due to viscous stresses and normal magnetic traction are indeed small compared to the first term in Eq. (7) (which involves surface tension and interfacial curvature). On the other hand, it is also well known that the addition of small corrections into boundary conditions can be extremely important (see for instance Refs. [29,41]). This is reinforced by the results we present here, where the typical number of fingers and the finger competition dynamics are significantly affected by the small corrections added into the generalized pressure jump boundary condition [Eq. (7)].

III. LINEAR STABILITY ANALYSIS

We begin our study by using Eq. (8) to examine how the development of interfacial instabilities at early stages of the pattern evolution could be modified by the influence of both viscous stresses and external magnetic field. We emphasize that the contribution from magnetic stresses (magnetic normal traction) is intrinsically a nonlinear concern, and is not required in the linear stability analysis of the problem. Unless otherwise stated, we consider a destabilizing driving $\dot{b}(t) > 0$, and as in Refs. [10,15,17] we assume an exponentially increasing gap width $b(t) = \exp t$, such that $[\dot{b}(t)/b(t)] = 1$. This is precisely the ideal plate separation profile used in related adhesion probe-tack tests [22], since it provides a more uniform kinematics and nearly constant strain rate. At short times we have that $b \approx 1 + t$ which corresponds to the constant lifting velocity case with $\dot{b} = 1$.

Inspecting Eq. (9) for the linear growth rate $\lambda(n)$ we can gain further insight about the role of lifting, viscous stresses, magnetic field, and surface tension in determining the interface instability. As usual, the contribution coming from the surface tension term has a stabilizing nature (σ stabilizes modes of large n). It is also evident that the azimuthal magnetic field contribution N_B always tends to stabilize the interface. On the other hand, the lifting term proportional to $\dot{b}/b$ basically plays a destabilizing role.

From Eq. (9) we can also obtain some direct consequences on the n dependence of the linear growth rate.

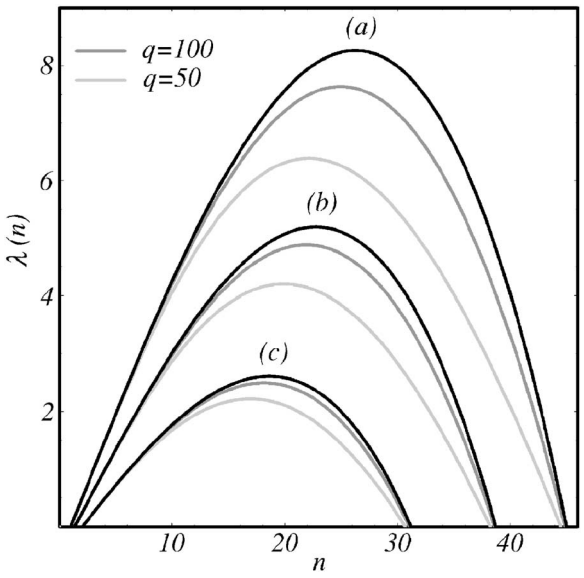

FIG. 2. Linear growth rate $\lambda(n)$ as a function of mode n, for $t = 0.2$, $\sigma = 1.5 \times 10^{-5}$, and three different values of N_B: (a) 0, (b) 3.5×10^{-3}, and (c) 7.0×10^{-3}. The color labeling refers to distinct values of δ and q: $\delta = 0$ (black), $\delta = 1$, $q = 100$ (dark gray), and $\delta = 1$, $q = 50$ (light gray).

For example, it can be verified that the mode $n = 0$, that corresponds to a uniform expansion of the circle, decays $[\lambda(0) = -1]$ for $\dot{b}(t) > 0$ as a consequence of mass conservation, and is marginal $[\lambda(0) = 0]$ for $\dot{b}(t) = 0$. In addition, the stability of mode $n = 1$, which corresponds to a rigid translation of the circular interface, is given solely by the magnetic term, so that it decays if $N_B > 0$, and is marginal if $N_B = 0$. This makes perfect sense, since the azimuthal magnetic field tends to attract the ferrofluid towards the current carrying wire, keeping the droplet pinned down at the center of the cell. For modes $n \geq 2$ the stability depends on the interplay of the three terms appearing in Eq. (9).

The unusual feature of Eq. (9) is the presence of the factor $J(n)$ [Eq. (10)], that introduces a dependency on the initial aspect ratio q. We recall that $J(n)$ arises directly from the inclusion of viscous stresses into the generalized pressure boundary condition [Eq. (7)]. However, the most interesting aspect of Eq. (9) is the fact that $J(n)$ appears as an overall prefactor, as well as a term multiplied by $\dot{b}(t)$, being inherently connected to the lifting itself. From Eq. (10) we see that, if $n \gg 1$ the correction incorporated by the term $J(n)$ is more important when $nb/qR \sim 1$. Of course, this explicit dependence with q completely disappears if the effect of normal stresses is not taken into account, so that $\delta = 0$, and $J(n) = 1$.

Figure 2 plots $\lambda(n)$ as a function of mode number n for a nonzero value of the surface tension parameter σ ($\sigma = 1.5 \times 10^{-5}$), $t = 0.2$, and for three different values of N_B: (a) 0, (b) 3.5×10^{-3}, and (c) 7.0×10^{-3}. The black curves correspond to the case in which normal viscous stresses are neglected ($\delta = 0$), and the gray curves refer to the cases in which such stresses are taken into account ($\delta = 1$). The gray color shading refers to the following values of the initial aspect ratio: q

=100 (dark gray), and $q=50$ (light gray). Unless otherwise stated this will be the color labeling used throughout this work.

The growth rate curves illustrated in Fig. 2 are characterized by a band of unstable modes of width

$$\Delta n_c = n_{c>} - n_{c<}, \tag{14}$$

where the critical mode $n_{c>}$ ($n_{c<}$) is the solution of a cubic equation, defined as the largest (smallest) wave number for which $\lambda(n)=0$. We point out that unlike the classical fingering problem in outward radial flow [3,4] and the centrifugally-driven problem in rotating Hele-Shaw cells [31,32], here the band of unstable modes shrinks from both ends ($n_{c>}$ and $n_{c<}$) due to the action of stabilizing effects.

Another common feature of such curves is the presence of a maximum at $n=n_{max}$, obtained by setting $d\lambda(n)/dn=0$. A quantity closely related to n_{max} is the so-called fastest growing mode n^*, defined as the *integer* mode that produces the largest growth rate. A given mode n is only the fastest growing when $\lambda(n)>\lambda(n-1)$ and $\lambda(n)>\lambda(n+1)$. This is the mode that will tend to dominate during the early stages of the pattern formation process and will perhaps determine the number of fingers in later stages.

By inspecting Fig. 2, we can examine how the magnetic field and the viscous stresses influence the linear growth rate when σ is nonzero: it is clear that increasingly larger values of N_B decrease the band of unstable modes Δn_c, and reduce the value of n_{max}. On the other hand, for a given value of N_B, changes in q do not affect Δn_c significantly. However, smaller values of q lead to a decreased growth rate of the mode n_{max}, shifting it toward lower values of azimuthal wave numbers. Since n_{max} determines the typical number of fingers formed at the onset of the instability, this means that small initial gaps (or equivalently, larger values of q) result in patterns with a larger number of fingers. This is an important consequence of the inclusion of normal viscous stresses in Eq. (7). So, if $\sigma\neq 0$ the emerging interfacial instabilities would be more effectively suppressed for larger values of N_B and smaller values of q. It is worth mentioning that if viscous stresses are neglected (black curves in Fig. 2) the values of n_{max} and $\lambda(n_{max})$ would be *overestimated*.

As commented in Sec. I, the number of fingers observed in experiments (with nonmagnetic fluids) at constant lifting velocity is considerably smaller than that predicted by traditional linear analysis which neglects normal viscous stresses and consider standard boundary conditions [26,27]. Recently, it has been shown [27] that the agreement between experiment and linear theory is improved, specially for large $b(t)$, if three-dimensional effects are taken into account. These 3D corrections are introduced considering the influence of wall wetting effects [41,42], which take into account the existence of a thin film of variable thickness separating the fingers from the plates. However, it has also been verified in Ref. [27] that for small $b(t)$ an important discrepancy still remains, despite the inclusion of 3D effects.

At this point, we suggest that a possible explanation for the decrease of the numbers of fingers when $b(t)$ is small found in Ref. [27], can be offered if we consider the effects of normal viscous stresses. As discussed throughout this section, the effects of these stresses are indeed more important for small $b(t)$, or equivalently for earlier times. At such early times, the instability has just set in, and our linear stability analysis (which now considers the effect of viscous stresses) should apply and be sufficiently accurate. A more quantitative account for this fact is depicted in Fig. 3, which plots the time evolution of n_{max} considering the typical experimental conditions used in Refs. [19,27], i.e., $R_0=20$ mm, $b_0=0.5$ mm, constant lifting velocity $V=\dot{b}=20\times 10^{-6}$ m/s, fluid viscosity $\eta=92$ Pa s, and surface tension $\gamma=18\times 10^{-3}$ N/m. By using these physical quantities we plot our Fig. 3 considering the corresponding dimensionless parameters: $\dot{b}=1$ and $\sigma=\gamma b_0^3/[12\eta|\dot{b}|(2R_0)^3]\approx 1.592\times 10^{-6}$. We also assume that there is no magnetic field applied ($N_B=0$), and consider earlier dimensionless times $0.15\leqslant t\leqslant 0.50$ (note that here the characteristic time $T=b_0/|\dot{b}|=25$). The black curve represents the situation in which viscous stresses are neglected ($\delta=0$), while the gray curve considers the effects of such stresses ($\delta=1$) for the exact value of the initial aspect ratio used in Ref. [27], i.e., $q=(2R_0/b_0)=80$. The open circles represent the experiemtal values obtained in Fig. 4 of Ref. [27]. By comparing the black and gray curves in Fig. 3 it is evident that viscous stresses (gray curve) reduce the number of fingers significantly, mostly at shorter times [or, for smaller $b(t)$]. It is also clear that the typical number of fingers is indeed *overestimated* if viscous stresses are *not* taken into account (black curve). In addition, by inspecting Fig. 3 we verify that the agreement between the experimen-

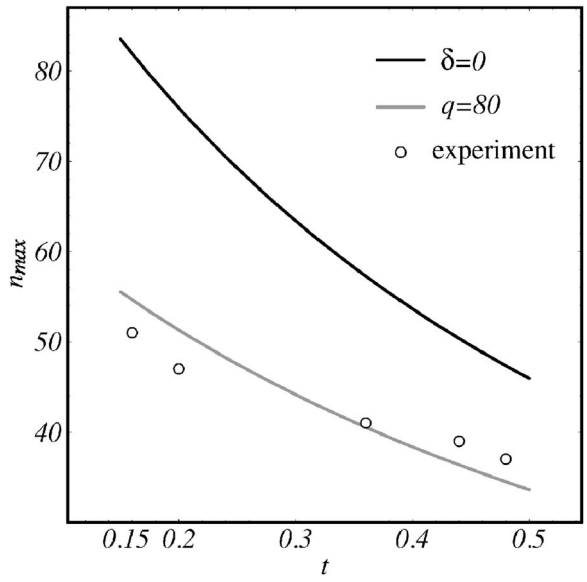

FIG. 3. n_{max} as a function of dimensionless time t, for lifting with constant velocity $\dot{b}=1$, $\sigma\approx 1.592\times 10^{-6}$, and $N_B=0$. These parameters match the experimental values presented in Refs. [19,27]. We plot the experimental data taken from Fig. 4 of Ref. [27] (open circles), and our corresponding linear stability results when $\delta=0$ (black curve), and $\delta=1$ with $q=80$ (gray curve). Note that the theoretical prediction for the typical number of fingers is considerably improved when viscous stresses are taken into account (gray curve).

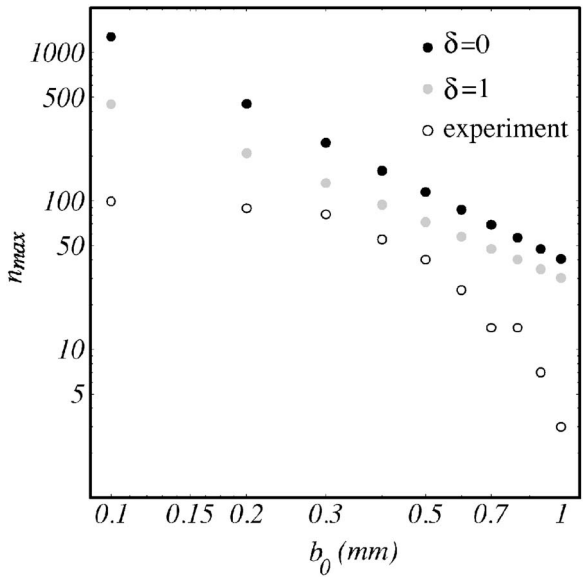

FIG. 4. Log-log plot depicting how the typical number of fingers n_{max} at time $t=0$ varies with initial plate spacing b_0 (0.1 mm$\leqslant b_0 \leqslant$1.0 mm). The physical parameters are the same as the ones used in Fig. 3. We plot the experimental data taken from Fig. 3 of Ref. [27] (open circles), and our corresponding linear stability results when $\delta=0$ (black dots), and $\delta=1$ (gray dots).

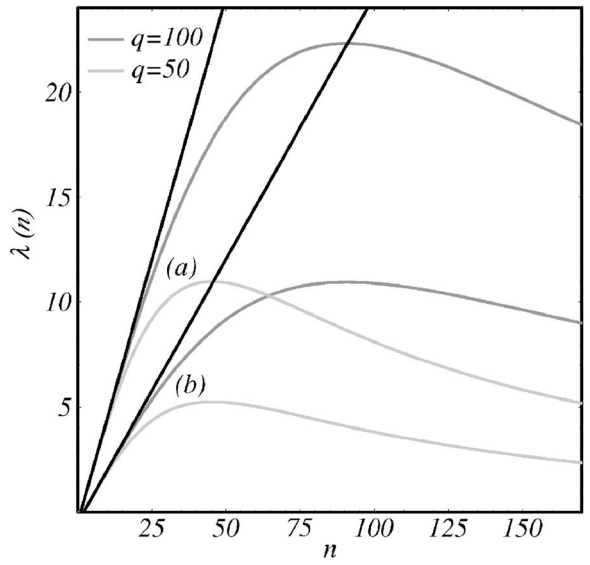

FIG. 5. Linear growth rate $\lambda(n)$ as a function of mode n, for $t=0.2$, $\sigma=0$, and two different values of N_B: (a) 0, and (b) 7.0×10^{-3}. The color labeling refers to distinct values of δ and q: $\delta=0$ (black), $\delta=1$, $q=100$ (dark gray), and $\delta=1$, $q=50$ (light gray).

tally observed number of fingers with the linear theoretical prediction is considerably improved when the effects of viscous stresses are considered.

To examine this issue a bit more systematically, in Fig. 4 we plot the typical number of fingers n_{max} at early times, for different values of the initial plate spacing b_0. As in Ref. [27] our theoretical data are calculated by assuming that $t=0$. Note that Fig. 4 uses the same set of physical parameters used in Fig. 3 (which was plotted for fixed $b_0=0.5$ mm), but now the time is fixed ($t=0$), and 0.1 mm$\leqslant b_0 \leqslant$1.0 mm. The data represented by the black (gray) dots assume that $\delta=0$ ($\delta=1$), and the open circles are the experimental data taken from Fig. 3 of Ref. [27]. By inspecting Fig. 4 we note that the gray dots ($\delta=1$) are always located below the black ones ($\delta=0$), indicating that the inclusion of viscous stresses leads to theoretical results which are closer to the experimental data for all measured values of b_0. Similarly to what we have already observed in Fig. 3, the effects of viscous stresses are indeed more relevant for smaller values of b_0. It can be seen that a better agreement between the theory including stress (gray dots) and the experiment (open circles) is obtained within the interval 0.2 mm$\leqslant b_0 \leqslant$0.6 mm. The deviation observed for larger b_0 is somewhat expected from the results of Ref. [27] (3D effects). Although we do not fully understand the persisting disagreement for *very small* plate spacings (0.1 mm$\leqslant b_0 \leqslant$0.2 mm), it could be possibly originated from the inherent inacurracy related to the experimental measurement of the number of fingers at very early times (here taken as $t=0$). We point out that an improved agreement between theory and experiment would be achieved, if the theoretical data would have been calculated by considering a small, but nonzero t. In summary, from the analysis of Figs. 3 and 4 it seems that in order to improve the agreement between linear theory and experiments [26,27] it is necessary to include not only three-dimensional effects [more relevant for larger $b(t)$], but also the effects of normal viscous stresses [important for intermediate and small $b(t)$]. In this sense, the inclusion of normal stresses we propose in this work add an important element into the discussion about the discrepancies observed in Refs. [26,27].

Now we analyze the growth rate considering the situation in which the surface tension parameter is set to zero (see Fig. 5). Throughout this work, the zero surface tension limit will be particularly useful, since it desensitizes the system with respect to σ, and allows a clearer elucidation of the role played by viscous stresses and magnetic field. Figure 5 plots the linear growth rate as a function of mode number, when $\sigma=0$, $t=0.2$, N_B:(a) 0, and (b) 7.0×10^{-3}. The value of the other physical parameters and the color coding are exactly the same as the ones employed in Fig. 2. When viscous stresses are neglected [back straight lines in both (a) and (b)] we notice that $\lambda(n)$ scales with n, and the system is ill posed [$\lambda(n)$ is unbounded for $n\rightarrow\infty$], regardless of the value of N_B. In other words, even though the slope of the straight lines are reduced for larger values of N_B, the growth rate curves will never present a well defined, finite peak (maximum) at a finite n if $\delta=0$. So, the magnetic effect alone is not enough to fully regularize the system at the linear stage, and N_B would not have any influence in determining n_{max} if $\sigma=0$ and $\delta=0$.

A completely different scenario is revealed when the effect of viscous stresses is taken into account: when $\delta=1$ [gray curves in both Figs. 5(a) and 5(b)], higher modes are stabilized, such that the curves present a well defined, finite n_{max} and a wide (but finite) Δn_c. Notice that, for a given N_B, smaller values of q (light gray curves) lead to lower values of both n_{max} and Δn_c. Interestingly, the position (along the n axis) of the peaks of the gray curves having the same q seem

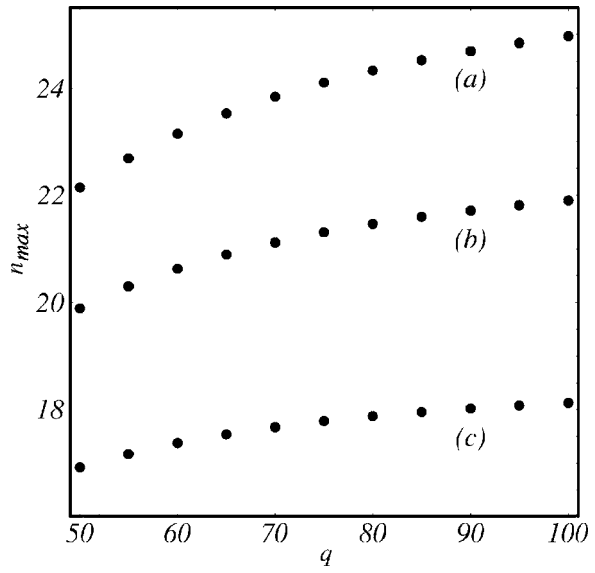

FIG. 6. n_{max} as a function of the initial aspect ratio q, for $t=0.2$, $\sigma=1.5\times10^{-5}$, $\delta=1$, and three different values of of N_B: (a) 0, (b) 3.5×10^{-3}, and (c) 7.0×10^{-3}. These physical parameters are the same as the ones used in Fig. 2.

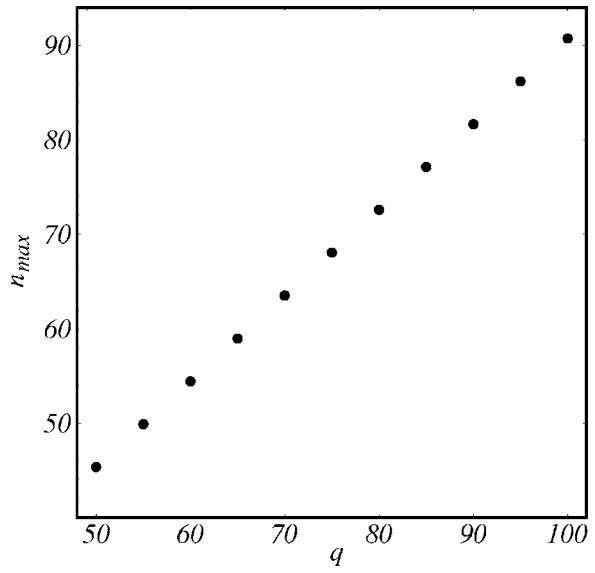

FIG. 7. n_{max} as a function of the initial aspect ratio q, for $t=0.2$, $\sigma=0$, $\delta=1$, and three different values of N_B: 0, 3.5×10^{-3}, and 7.0×10^{-3}. Note that hidden in the simple dotted line there are in fact three lines (one for each value of N_B). These physical parameters are the same as the ones used in Fig. 5.

to coincide. As we have anticipated, the value of n_{max} does not seem to depend on N_B, but solely on q. Therefore, the existence of a peak in the gray curves of Fig. 5 is due exclusively to the action of viscous stresses. In this sense, the inclusion of normal stresses ($\delta=1$) in the modified pressure boundary condition Eq. (7) introduces an effective surface tension into the system. Hence, within the scope of the linear theory, we conclude that the combined action of magnetic field and normal viscous stresses could be used as control parameters to discipline the emergence of interfacial instabilities.

To investigate more closely the combined influence of the magnetic field and viscous stresses on the mode of largest growth rate, in Fig. 6 we plot n_{max} as a function of q, for three different values of N_B, $\delta=1$, $t=0.2$, and $\sigma=1.5\times10^{-5}$. The values of N_B are exactly the same ones as those used in Fig. 2. By examining Fig. 6 we observe that $n_{max}$is more sensitive to changes in q for smaller values of N_B. By increasing q in Fig. 6, the typical number of fingers increases by approximately three units in (a) for $N_B=0$, two units in (b) for $N_B=3.5\times10^{-3}$, and roughly by one unit in (c) for $N_B=7.0\times10^{-3}$. Actually, this is the trend for any time t: we have verified that n_{max} is a decreasing function of time, decaying more rapidly for smaller values of q, and larger values of N_B.

We have also observed that, if σ is decreased, n_{max} varies much more dramatically with q while the three different dotted curves originally shown in Fig. 6 tend to coincide when $\sigma\to0$. With respect to this last point, observe Fig. 7 which plots n_{max} as a function of q, when $\sigma=0$ and $\delta=1$: we note that hidden in the dotted straight line depicted in Fig. 7 there are in fact three dotted lines (two other indistinguishable dotted lines lie hidden). This reinforces our claim (see discussion of Fig. 5) that N_B has no influence in determining n_{max} as σ is set to zero. Indeed, if $\sigma=0$ and we calculate $d\lambda(n)/dn=0$, the terms involving N_B cancel out, and it can be shown that

$$n_{max}=\sqrt{\frac{6}{\delta}\frac{R}{b}}q. \tag{15}$$

From Eq. (15) we see that n_{max} varies linearly with q, and as expected, tends to infinity when $\delta\to0$ since in this limit $\lambda(n)$ is unbounded. However, if $\delta=1$, n_{max} is a decreasing function of time, indicating that, due to viscous stresses, the droplet would tend to recircularize even if both σ and N_B are zero.

Complementary information can be obtained by examining Fig. 8 which uses the same physical parameters as the ones utilized in Fig. 6, but depicts a "phase diagram" in N_B-q parameter space for the linearized system. The curves that encompass the various shaded regions, determined from the condition

$$\lambda(n)=\lambda(n\pm1), \tag{16}$$

denote zones where a particular mode is the fastest growing. These zones are labeled by n^* on the graph. As an example of how one might use this graph, consider the case where $N_B=3.5\times10^{-3}$ is held fixed. When the initial aspect ratio increases from $q=50$ to $q=100$, the fastest growing mode also increases, varying from $n^*=20$ to $n^*=22$. In addition, notice that as N_B is increased the shaded regions narrow and become more horizontally oriented, indicating that the influence of q is weak for higher magnetic Bond numbers. On the other hand, if q is held fixed (for example, $q=100$), as N_B is increased, we see that the fastest growing mode decreases, changing from $n^*=25$ to $n^*=18$. These findings are in perfect agreement with what we have observed in Fig. 6 for three particular values of N_B. We have also verified that when $\sigma\to0$ the boundary regions for each n^* become very narrow

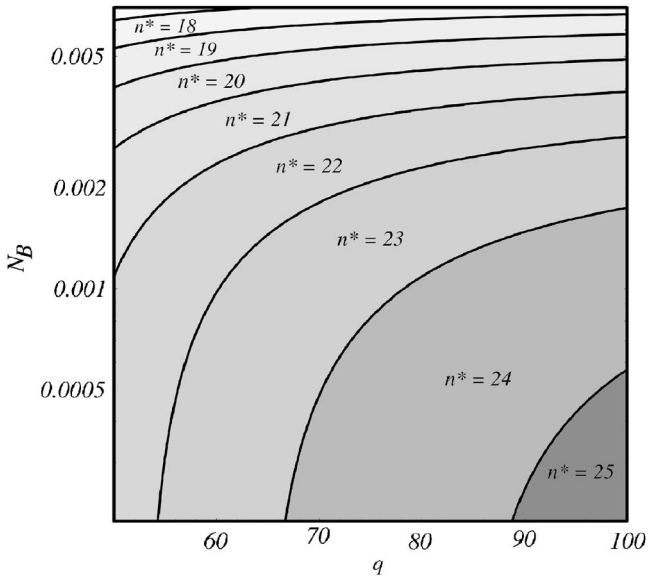

FIG. 8. Log-linear plot of the linear stability phase diagram showing zones (shaded) of fastest growing mode n^* as given by Eq. (16). The physical parameters are exactly the same as the ones used in Fig. 2.

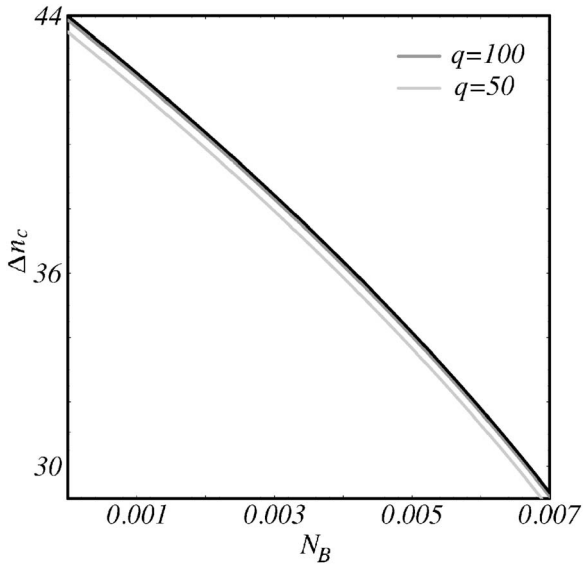

FIG. 9. Width of the band of unstable modes Δn_c as a function of the magnetic Bond number N_B when $\sigma \neq 0$: $\delta=0$ (black), $\delta=1$, $q=100$ (dark gray), and $\delta=1$, $q=50$ (light gray). The physical parameters are exactly the same as the ones used in Fig. 2.

stripes directed along the vertical axis (or, along the N_B axis), in such a way that changes in N_B have no influence whatsoever in the values of n^*, confirming the collapse of curves we have detected in Fig. 7.

Interestingly, despite the evident dependence of the fastest growing mode n^* (or, n_{max}) on both q and N_B when $\sigma \neq 0$, as indicated in Figs. 2 and 6, it can be observed that the band of unstable modes Δn_c decreases for increasing N_B, but for a given N_B, is very weakly influenced by changes in the initial gap spacing (or, by changes in q). This fact can be very clearly verified in Fig. 9, which depicts how Δn_c changes with N_B, for $q=100$ (dark gray curve), $q=50$ (light gray curve), and when $\delta=0$ (black curve). In contrast, when surface tension is zero and $\delta=1$ (see Fig. 10), the band of unstable modes is much more sensitive to changes in q. Moreover, it can be verified that Δn_c changes more significantly with N_B for larger values of q. Again, in the zero surface tension limit we can have analytical access to another important quantity, namely the critical value of the magnetic Bond number required to stabilize all modes

$$N_{Bc} = \frac{R^4 \dot{b}}{2b^3}\left[1 - \sqrt{\frac{\delta}{6}}\frac{b}{qR}\right]^2. \tag{17}$$

From Eq. (17) it is clear that when viscous stresses are considered ($\delta=1$) and q is small, a smaller N_{Bc} is required to stabilize all the modes. It is also worth noting that N_{Bc} is a decreasing function of time. This suggests that, as time progresses, droplet recircularization would be favored, even if $\sigma=0$.

IV. WEAKLY NONLINEAR DYNAMICS

In the previous section, we have verified that the linear analysis can be very useful in describing important aspects related to the stability of the fluid-fluid interface, mainly the ones related to the typical number of fingers formed, and the critical magnetic field needed to stabilize all interfacial modes. In this section, we turn our attention to the weakly nonlinear, intermediate stages of pattern evolution. Now we are not only interested in interface stability issues, but also to access important morphological features of the patterns formed in lifting Hele-Shaw cells.

As discussed in the Introduction of this paper (Sec. I), the most noteworthy morphological aspect for pattern formation in lifting Hele-Shaw flow is the strong competition among

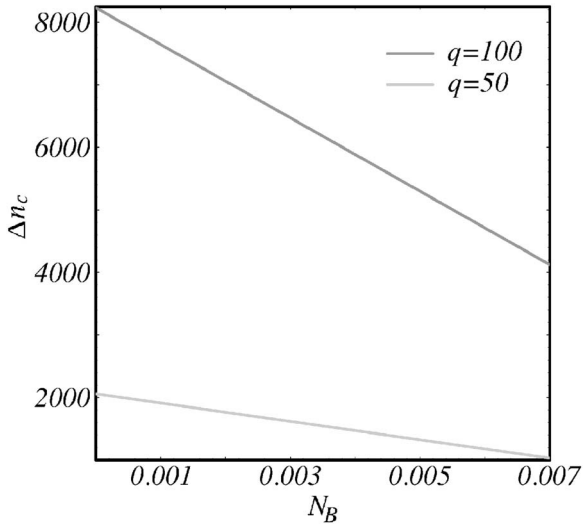

FIG. 10. Width of the band of unstable modes Δn_c as a function of the magnetic Bond number N_B when $\sigma=0$: $\delta=1$, $q=100$ (dark gray), and $q=50$ (light gray). The physical parameters are exactly the same as the ones used in Fig. 5. There is no black curve ($\delta=0$) since in this case $\Delta n_c \to \infty$.

the penetrating fingering structures, while the competition among the fingers of the more viscous fluid is considerably less intense. Our main goal is to get analytical insight about such finger competition process both in zero and nonzero surface tension circumstances, when the combined action of normal stresses and magnetic field are considered. The purely nonlinear effects introduced by the magnetic normal traction $[\mu_0(\mathbf{M}\cdot\mathbf{n})^2]/2$ [second term on the right hand side of Eq. (7)] are also examined.

The second order mode-coupling approach executed here has been quite successful in accurately describing finger competition mechanisms arising in radial Hele-Shaw cells with injection [4] and also in rotating Hele-Shaw flow [30]. Recent numerical results [48] substantiate the analytical predictions of Ref. [30], providing a convincing evidence of the usefulness of the weakly nonlinear description. Within our weakly nonlinear approach, finger competition is related to the influence of a fundamental mode n, assuming n is even, on the growth of its subharmonic mode $n/2$ [4,30]. To simplify our discussion it is convenient to rewrite the net perturbation ζ in terms of cosine $[a_n=\zeta_n+\zeta_{-n}]$ and sine $[b_n=i(\zeta_n-\zeta_{-n})]$ modes. Without loss of generality we may choose the phase of the fundamental mode so that $a_n>0$ and $b_n=0$. From Eq. (8) we obtain the equations of motion for the subharmonic mode

$$\dot{a}_{n/2}=\{\lambda(n/2)+C(n)a_n\}a_{n/2}, \tag{18}$$

$$\dot{b}_{n/2}=\{\lambda(n/2)-C(n)a_n\}b_{n/2}, \tag{19}$$

where the function

$$C(n)=\frac{1}{2}\left[F\left(-\frac{n}{2},\frac{n}{2}\right)+\lambda(n/2)G\left(\frac{n}{2},-\frac{n}{2}\right)\right] \tag{20}$$

regulates finger competition behavior.

In Fig. 11 we plot $C(n)$ as a function of time for two values of n, when $\sigma=1.5\times10^{-5}$. The solid (dashed) curves describe the behavior of $C(n)$ in the absence (presence) of the magnetic field. The nonzero $N_B=2.0\times10^{-4}$ and $\chi=5$. The black (gray) curves assume that the normal stress parameter $\delta=0$ ($\delta=1$). Light (dark) gray curves refer to $q=50$ ($q=100$). It is clear from Fig. 11 that $C(n)\leqslant 0$. From Eqs. (18) and (19) we verify that a negative $C(n)$ increases the growth of the sine subharmonic $b_{n/2}$, while inhibiting growth of its cosine subharmonic $a_{n/2}$. The result is an increased variability among the lengths of fingers of the outer fluid penetrating into the ferrofluid. This effect describes the competition of inward fingers. We stress this is in line with what is observed in experiments [19–21,25,26] and numerical simulations [10] of the lifting flow problem with nonmagnetic fluids.

At intermediate stages of pattern evolution, the question arises as whether viscous stresses play a relevant role in the finger competition dynamics. To examine this issue, first we focus on the situation in which there is no applied magnetic field (solid curves in Fig. 11). If $N_B=0$ we see that the curves representing $C(n)$ behave differently if the influence of viscous stresses is taken into account: for a given n, we see that the curve associated to smaller q lies on the top of the other two. This indicates that finger competition would be less

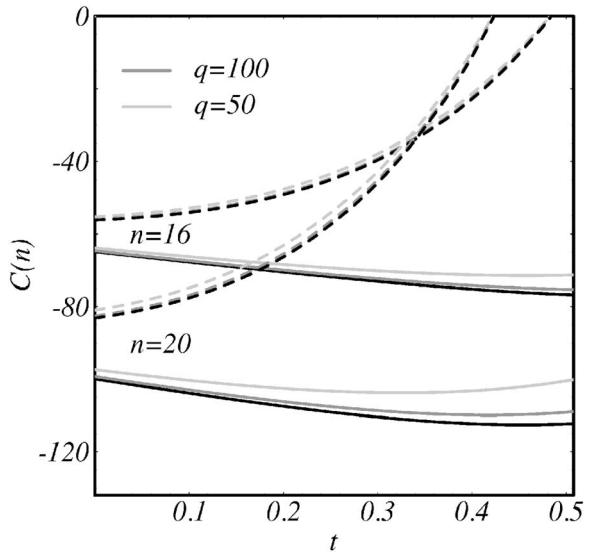

FIG. 11. $C(n)$ as a function of time for modes $n=16$ and $n=20$ in the nonzero surface tension case ($\sigma=1.5\times10^{-5}$). The black (gray) curves refer to $\delta=0$ ($\delta=1$). The magnetic Bond number is $N_B=0$ ($N_B=2.0\times10^{-4}$) for the solid (dashed) curves, $q=50$ (light gray curves), and $q=100$ (dark gray curves). The magnetic susceptibility $\chi=5$. Note that the initial aspect ratio q comes into play only when $\delta=1$.

intense for lower values of the initial aspect ratio q. So, the harder the spatial confinement set at $t=0$, the harder the competition at later times. This theoretical finding is in agreement with the experimental observations for stretch-flow of immiscible (nonmagnetic) Newtonian fluids [19,26,27]. In such experiments, little (strong) fingering and competition are observed for large (small) initial plate spacing. The dependence of the finger competition dynamics on q is another important consequence of the introduction of normal stresses into the lifting Hele-Shaw cell problem.

Despite the important connection between finger competiton and q discussed in the previous paragraph, it is worth noting that, the combined effect of normal stresses and surface tension is not quite enough to make $C(n)\to 0$ within the typical time scales for which our theory is quantitatively accurate. A distinct behavior is observed when the magnetic field is nonzero (dashed curves in Fig. 11): $C(n)$ is negative and increases as time advances. Eventually, $C(n)$ vanishes meaning that the competition ceases due to the action of the magnetic field. Although normal stresses may contribute to restrain competition of inward fingers when $N_B\neq 0$, they do not have a major role in setting the time for which competition vanishes. This can be verified by the fact that, for a given n, all dashed curves tend to coincide when $C(n)\to 0$. It is also interesting to observe that competition goes to zero first for mode $n=20$, making the dashed curves for $n=16$ and $n=20$ to cross one another before they reach the $C(n)=0$ line.

In Fig. 12 we plot $C(n)$ as a function of t, but now we assume that $\sigma=0$. All remaining physical parameters are identical to those used in Fig. 11. By inspecting Fig. 12 we note that when $N_B=0$ (solid curves), $C(n)$ is a monotonically decreasing function of time. By comparing the solid curves

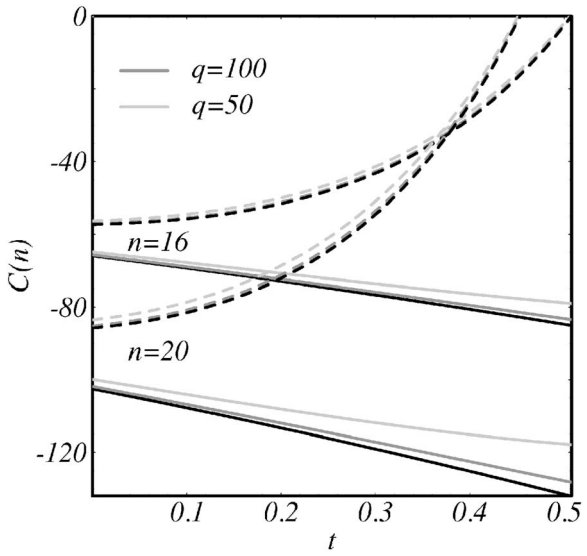

FIG. 12. $C(n)$ as a function of time for modes $n=16$ and $n=20$ in the zero surface tension case. The black (gray) curves refer to $\delta=0$ ($\delta=1$). The magnetic Bond number is $N_B=0$ ($N_B=2.0\times10^{-4}$) for the solid (dashed) curves, $q=50$ (light gray curves), and $q=100$ (dark gray curves). The magnetic susceptibility $\chi=5$. Note that the initial aspect ratio q comes into play only when $\delta=1$.

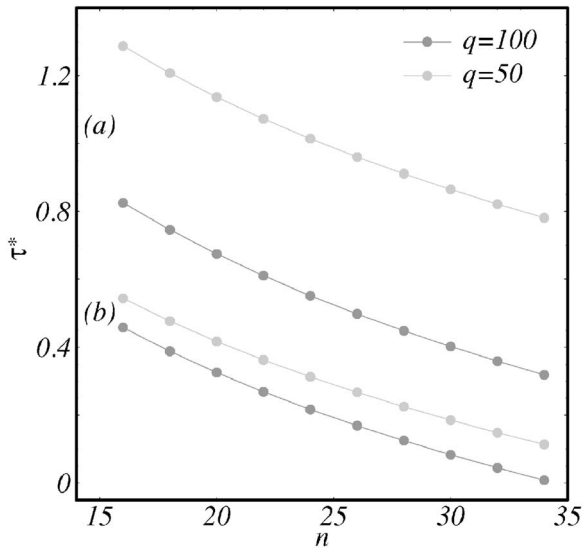

FIG. 13. Dimensionless time τ^* for which the strength of finger competition is largest (in the absence of a magnetic field) as a function of mode n, when (a) $\sigma=0$ (see Fig. 12), (b) $\sigma=1.5\times10^{-5}$ (see Fig. 11). We consider that $q=100$ (dark gray) and $q=50$ (light gray).

plotted in Figs. 11 and 12, one clearly observes that the absence of surface tension is responsible for such a behavior. This would favor an ever increasing competition among the inward fingers. However, it is important to point out that, although surface tension is completely absent in Fig. 12, normal stresses still act to decrease the intensity of the finger competition (solid curves move upwards for smaller q).

Similarly to the nonzero surface tension case illustrated in Fig. 11, the situation is changed when an external magnetic field is applied. By observing the dashed curves in Fig. 12 we see that they go to zero at a given time, indicating that competition vanishes, despite the fact that $\sigma=0$. As expected, by comparing Figs. 11 and 12 we conclude that the required time to suppress competition is smaller when surface tension is nonzero. This is clearly verified by noting that the zeros of the dashed $C(n)$ curves are shifted to the left in Fig. 11.

In order to analyze in greater detail other relevant aspects of the finger competition dynamics in the lifting Hele-Shaw setup, we conclude this section by analyzing Figs. 13 and 14. Figure 13 summarizes the influence of viscous stresses on finger competition both in the absence (a) and presence (b) of surface tension. For both values of surface tension, we consider two different values of the initial aspect ratio: $q=100$ (dark gray) and $q=50$ (light gray). We focus on the case in which $N_B=0$, and plot the dimensionless time τ^* at which the finger competition function $C(n)$ assumes its largest magnitude (minima of the solid gray curves in Figs. 11 and 12), as a function of mode n. Indeed, we verify that finger competition can be significantly affected by the sole action of viscous stresses. When surface tension is zero [Fig. 13(a)] we note that, for a given n, τ^* is smaller for higher initial confinement (larger q). It is evident that, the lifting system is strongly dependent on the initial conditions, in the sense that changes in q lead to important variations in the finger competition dynamics. It is also observed that τ^* is a decreasing function of mode n, indicating that finger competition is stronger at relatively early stages of the lifting process, when higher modes n are manifestly unstable. All these remarks are also valid for the nonzero surface tension case [Fig. 13(b)], but from the fact that curves for different q are closer to each other, it is obvious that the existence of interfacial tension (which stabilizes modes of large n) decreases the

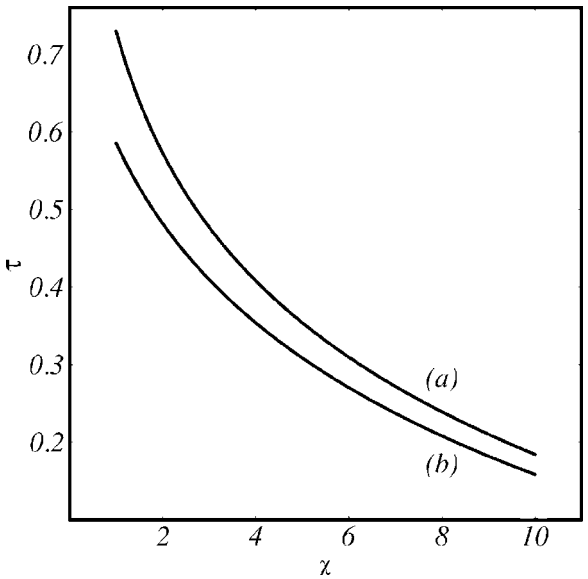

FIG. 14. Dimensionless time τ for which $C(n)=0$, as a function of magnetic susceptibility χ ($1\leqslant\chi\leqslant10$), when (a) $\sigma=0$, (b) $\sigma=1.5\times10^{-5}$, for $n=30$, $N_B=2.0\times10^{-4}$, and $\delta=0$. The remaining physical parameters are the same is the ones used in Figs. 11 and 12.

sensitivity of the system with respect to changes in q.

We proceed by examining Fig. 14. Here we intend to investigate a bit more closely the influence of the purely nonlinear contribution coming from the magnetic normal traction [second term on the right hand side of Eq. (7)], which introduced an explicit dependence of the mode-coupling term $F(n,n')$ on the magnetic susceptibility χ [last term in Eq. (12)]. Figure 14 depicts the time τ at which all finger competition is suppressed [zeros of $C(n)$ for $N_B \neq 0$] as a function of magnetic susceptibility χ, for both (a) zero and (b) nonzero surface tension ($\sigma = 1.5 \times 10^{-5}$) cases. Without loss of generality we assume that $n=30$ and $N_B = 2.0 \times 10^{-4}$, and use the same physical parameters employed in Figs. 11 and 12. Since the influence of normal viscous stresses is negligible to determine τ, Fig. 14 is plotted by assuming that $\delta=0$.

Figure 14 clearly illustrates that, regardless the value of σ, the time τ required to completely suppress finger competition is strongly dependent on the value of the magnetic susceptibility, becoming significantly smaller as χ is increased. At first, this dependence may seem too obvious. However, we note in passing that the value of the magnetic Bond number used throughout this weakly nonlinear Sec. IV is one order of magnitude smaller than the typical values of N_B utilized in the linear study carried out in Sec. III. This is possible due to the inclusion of the magnetic normal traction in Eq. (7). Now one can afford using a considerably lower value of N_B and still completely restrain finger competition by tuning the value of the magnetic susceptibility. In other words, even if N_B is kept fixed, one might determine the typical time for which finger competition should be suppressed, by appropriately selecting the value of χ. We can gain additional insight about this last point by analyzing the expression of the magnetic Bond number which is required to suppress finger competition entirely (for simplicity we assume that $\sigma=0$ and $\delta=0$)

$$\bar{N}_B = \left(\frac{4n+2}{\chi n^2 + 4n + 10} \right) N_{Bc}, \tag{21}$$

obtained from Eq. (20) by setting $C(n)=0$. In Eq. (21) N_{Bc} denotes the critical magnetic Bond number required to stabilize all interfacial modes at *linear* stages [see Eq. (17)], while $\bar{N}_B$ is a legitimately *nonlinear* concept. From Eq. (21) we notice that the magnetic Bond number $\bar{N}_B$ at which competition is fully suppressed can be indeed significantly smaller than the critical (linear) Bond number N_{Bc}, mainly for larger values of χ and n. This dependence of $\bar{N}_B$ on χ is a direct and important consequence of the introduction of the magnetic normal traction term in the generalized Young-Laplace pressure jump boundary condition [Eq. (7)]. This purely nonlinear magnetic contribution provides an additional support to the idea of conveniently controlling interfacial instabilities and singularities in lifting Hele-Shaw cells by magnetic means [16,24].

V. CONCLUDING REMARKS

In this work we studied various aspects related to pattern formation in lifting Hele-Shaw cells both in the purely linear, and during intermediate nonlinear stages of interface evolution. Our analytical approach incorporates the combined role of three relevant parameters for the problem, namely the viscous stresses (accounted when $\delta=1$), the applied magnetic field (N_B), and the surface tension (σ). In particular, we have explored the fact that the inclusion of viscous stresses into the problem leads to a pertinent dependence of the system on the initial aspect ratio q at both linear and nonlinear stages. At the nonlinear level, a fourth relevant parameter (the magnetic susceptibility χ) is revealed, resulting from the action of magnetic stresses (magnetic normal traction) at the interface.

At the linear stage, if $\sigma=0$ it is verified that viscous stresses regularize the system, working as an effective surface tension. In this case the initial aspect ratio q influences both the typical number of fingers n_{max} and the band of unstable modes Δn_c: Δn_c changes more significantly with N_B for larger q, but n_{max} does not depend on N_B, but solely on q. If $\sigma \neq 0$, we have shown that the typical number of fingers is quite influenced by q, while Δn_c does not change as much. When radial viscous stresses are considered we find the number of emerging fingers to be considerably smaller than the predicted by usual linear stability analyses which neglect such stresses. This last theoretical finding is supported by experimental results in lifting Hele-Shaw flows with nonmagnetic fluids [19,27]. This indicates that the inclusion of viscous stresses add an important element to elucidate recent discrepancies between other theoretical models (which neglect viscous stresses) and experiments on the typical number of fingers [26,27].

At the weakly nonlinear stage, we focus on the influence of δ and N_B on the competition among fingering structures. We have found that normal stresses significantly affect finger competition dynamics, leading to an interesting connection between the initial aspect ratio and the strength of the competition: if the system is highly confined at $t=0$ (larger q) the competition at later times is expected to be quite strong as well. Therefore, we have shown that the inclusion of viscous stresses is of considerable importance for an accurate description of the lifting problem. We have also identified the specific role played by N_B and δ: while viscous stresses act to restrain or delay the occurrence of finger competition, the magnetic field is able to suppress it completely. The intrinsically nonlinear effect introduced by the magnetic normal traction in the generalized pressure boundary condition [Eq. (7)] has also been examined. It revealed the key role played by the magnetic susceptibility χ in the control mechanism of the finger competition dynamics. We have found that by choosing an appropriate ferrofluid (that is, by tuning χ), one can presumably control the fingering development by using magnetic Bond numbers which are far smaller in magnitude than those typically predicted by linear stability theory. In this context, the combined action of normal viscous stresses, magnetic normal traction, and magnetic field conspire to inhibit the formation of interfacial instabilities if $\sigma \neq 0$, and to prevent interfacial singularities when $\sigma=0$.

The fact that normal (viscous and magnetic) stresses and azimuthal magnetic field restrain fingering formation in stretch flow may have important implications on the evaluation of adhesiveness and peel-off forces of a given liquid adhesive material. It has been recently shown [24], under constant drive speed conditions and by neglecting effects of fingering, that the net effect of an azimuthal magnetic field would be to reduce adhesion. A natural extension of the current work is to investigate the role of normal stresses, magnetic field, and fingering in possibly influencing the adhesion properties of confined fluids both under constant load [13] and constant lifting velocity [18–21,25,26] circumstances.

ACKNOWLEDGMENTS

We thank CNPq (Brazilian Research Council) for financial support of this research through the CNPq/FAPESQ Pronex program. J.A.M. thanks CNPq for financial support (PDE Proceeding No. 200045/2005-9). We acknowledge useful discussions with Enrique Alvarez-Lacalle and Jaume Casademunt. We thank Daniel Bonn and Martine Ben Amar for kindly supplying the experimental data of Ref. [27].

[1] P. G. Saffman and G. I. Taylor, Proc. R. Soc. London, Ser. A **245**, 312 (1958).
[2] G. M. Homsy, Annu. Rev. Fluid Mech. **19**, 271 (1987) K. V. McCloud and J. V. Maher, Phys. Rep. **260**, 139 (1995).
[3] L. Paterson, J. Fluid Mech. **113**, 513 (1981).
[4] J. A. Miranda and M. Widom, Physica D **120**, 315 (1998).
[5] T. Vicsek, *Fractal Growth Processes* (World Scientific, Singapore, 1989).
[6] E. Ben-Jacob, R. Godbey, N. D. Goldenfeld, J. Koplik, H. Levine, T. Mueller, and L. M. Sander, Phys. Rev. Lett. **55**, 1315 (1985).
[7] H. La Roche, J. F. Fernández, M. Octavio, A. G. Loeser, and C. J. Lobb, Phys. Rev. A **44**, R6185 (1991).
[8] A. A. Sonin and R. Bartolino, Nuovo Cimento D **15**, 1 (1993).
[9] S.-Z. Zhang, E. Louis, O. Pla, and F. Guinea, Eur. Phys. J. B **1**, 123 (1998).
[10] M. J. Shelley, F.-R. Tian, and K. Wlodarski, Nonlinearity **10**, 1471 (1997).
[11] J. Bohr, S. Brunak, and T. Norretranders, Europhys. Lett. **25**, 245 (1994).
[12] S. Roy and S. Tarafdar, Phys. Rev. E **54**, 6495 (1996).
[13] S. K. Thamida, P. V. Takhistov, and H.-C. Chang, Phys. Fluids **13**, 2190 (2001).
[14] S. Sinha, S. K. Kabiraj, T. Dutta, and S. Tarafdar, Eur. Phys. J. B **36**, 297 (2003).
[15] S. K. Kabiraj and S. Tarafdar, Physica A **328**, 305 (2003).
[16] J. A. Miranda and R. M. Oliveira, Phys. Rev. E **69**, 066312 (2004).
[17] C.-Y. Chen, C.-H. Chen, and J. A. Miranda, Phys. Rev. E **71**, 056304 (2005).
[18] B. A. Francis and R. G. Horn, J. Appl. Phys. **89**, 4167 (2005).
[19] D. Derks, A. Lindner, C. Creton, and D. Bonn, J. Appl. Phys. **93**, 1557 (2003).
[20] S. Poivet, F. Nallet, C. Gay, and P. Fabre, Europhys. Lett. **62**, 244 (2003).
[21] M. Tirumkudulu, W. B. Russel, and T. J. Huang, Phys. Fluids **15**, 1588 (2003).
[22] R. D. Welsh, M.Sc. thesis, Massachusetts Institute of Technology, 2001.
[23] J. A. Miranda, Phys. Rev. E **69**, 016311 (2004).
[24] J. A. Miranda, R. M. Oliveira, and D. P. Jackson, Phys. Rev. E **70**, 036311 (2004).
[25] S. Poivet, F. Nallet, C. Gay, J. Teisseire, and P. Fabre, Eur. Phys. J. E **15**, 97 (2004).
[26] A. Lindner, D. Derks, and M. J. Shelley, Phys. Fluids **17**, 072107 (2005).
[27] M. Ben Amar and D. Bonn, Physica D **209**, 1 (2005).
[28] D. Korteweg, Arch. Neerl. Sci. Exactes Nat. Ser. II **6**, 1 (1901).
[29] E. Alvarez-Lacalle, J. Ortín, and J. Casademunt, Phys. Fluids **16**, 908 (2004).
[30] H. Gadêlha and J. A. Miranda, Phys. Rev. E **70**, 066308 (2004).
[31] L. W. Schwartz, Phys. Fluids A **1**, 167 (1989).
[32] L. Carrillo, F. X. Magdaleno, J. Casademunt, and J. Ortín, Phys. Rev. E **54**, 6260 (1996).
[33] R. E. Rosensweig, *Ferrohydrodynamics* (Cambridge University Press, Cambridge, 1985), and references therein.
[34] E. Blums, A. Cebers, and M. M. Maiorov, *Magnetic Fluids* (de Gruyter, New York, 1997), and references therein.
[35] J. A. Miranda, Phys. Rev. E **62**, 2985 (2000).
[36] D. P. Jackson and J. A. Miranda, Phys. Rev. E **67**, 017301 (2003).
[37] A. O. Tsebers and M. M. Maiorov, Magnetohydrodynamics (N.Y.) **16**, 21 (1980).
[38] S. A. Langer, R. E. Goldstein, and D. P. Jackson, Phys. Rev. A **46**, 4894 (1992).
[39] D. P. Jackson, R. E. Goldstein, and A. O. Cebers, Phys. Rev. E **50**, 298 (1994).
[40] A. O. Cebers, Magnetohydrodynamics (N.Y.) **17**, 113 (1981).
[41] C.-W. Park and G. M. Homsy, J. Fluid Mech. **139**, 291 (1984).
[42] D. A. Reinelt, J. Fluid Mech. **183**, 219 (1987).
[43] L. D. Landau, E. M. Lifshitz, *Course of Theoretical Mechanics: Fluid Mechanics*, Vol. 6 (Pergamon Press, New York, 1959).
[44] G. Tryggvason and H. Aref, J. Fluid Mech. **136**, 1 (1983).
[45] H. C. Brinkman, Appl. Sci. Res., Sect. A **1**, 27 (1947).
[46] J. Fernandez, P. Kurowski, P. Petitjeans, and E. Meiburg, J. Fluid Mech. **451**, 239 (2002).
[47] J. Zeng and Y. C. Yortsos, Phys. Fluids **15**, 3829 (2003).
[48] J. A. Miranda and E. Alvarez-Lacalle, Phys. Rev. E **72**, 026306 (2005).